

RSC Advances



This is an *Accepted Manuscript*, which has been through the Royal Society of Chemistry peer review process and has been accepted for publication.

Accepted Manuscripts are published online shortly after acceptance, before technical editing, formatting and proof reading. Using this free service, authors can make their results available to the community, in citable form, before we publish the edited article. This *Accepted Manuscript* will be replaced by the edited, formatted and paginated article as soon as this is available.

You can find more information about *Accepted Manuscripts* in the [Information for Authors](#).

Please note that technical editing may introduce minor changes to the text and/or graphics, which may alter content. The journal's standard [Terms & Conditions](#) and the [Ethical guidelines](#) still apply. In no event shall the Royal Society of Chemistry be held responsible for any errors or omissions in this *Accepted Manuscript* or any consequences arising from the use of any information it contains.

Analysis of contact area between water and irregular fibrous surface for prediction of wettability

Yue Yuan,¹ Seong-O Choi,^{2,3} and Jooyoun Kim^{1,4*}

¹Department of Apparel, Textiles, and Interior Design, Kansas State University, Manhattan, KS, USA

²Department of Anatomy and Physiology

³Nanotechnology Innovation Center of Kansas State

⁴Johnson Cancer Research Center, Kansas State University, Manhattan, KS, USA

To Whom Correspondence should be addressed: Jooyoun Kim * jkim256@ksu.edu

Abstract

A characterization method, which allows a visual observation of the surface area that is wet by a liquid on a roughened surface, called as solid fraction (f_s) in the Cassie-Baxter model, was developed. To this end, superhydrophobic polystyrene (PS) webs (contact angles $\sim 170^\circ$, sliding angles $\sim 3^\circ$) were fabricated via electrospinning and subsequent coating with perfluorodecyltrichlorosilane (PFDTs). The theoretical solid fraction of the Cassie-Baxter model, f_s , was calculated by the equation with the measured contact angles at the flat surface and the rough surface of electrospun webs. Microscopic images of the PS webs were converted into black and white binary images after adjusting the gray-scale of the images to match the bright area fraction with the theoretical f_s . For visual observation of actual solid fraction, a drop of aqueous solution with hydrophobic fluorescent dye was rolled on the surface. The traces of the dye on the PS surface was analyzed by fluorescence microscopy to measure the actual solid fraction (f_s^{dye}) that was wet by the aqueous solution. f_s^{dye} corresponded well with the theoretical f_s , for the webs with superhydrophobic characteristics.

Keywords; superhydrophobicity, electrospinning, solid fraction f_s , fluorescence microscopy, contact angle

Introduction

Superhydrophobic surfaces have gained significant scientific and industrial interest for their potential applications to anti-fouling,¹ anti-fogging,² self-cleaning,³ and protective surfaces.⁴⁻⁵ A common design strategy for a superhydrophobic surface is to implement micro or nano-sized roughness onto a surface with low surface energy.⁶⁻¹² With an increased emphasis on forming the surface roughness to achieve a superhydrophobic surface, various fabrication methods have been employed to create surface roughness, including electrospinning,¹³⁻¹⁴ lithography,¹⁵ particle-deposition,¹⁶ plasma etching,^{11-12,17-18} and chemical etching.¹⁹ Among those methods, electrospinning is a convenient way to generate nano to micro-sized fibers with tunable morphology such as beads, pores and wrinkles.^{14,20}

Surface wettability or anti-wettability is generally represented by a static contact angle (CA) and/or a contact angle hysteresis. A surface with a high water contact angle (typically $>150^\circ$) and a low contact angle hysteresis (typically $<5^\circ$) is regarded as being superhydrophobic.^{6,21} For a flat surface, the contact angle is solely dependent on the surface energies of solid and liquid phases, as Young's equation²² defines. For a roughened surface, the presence of surface roughness can either increase or decrease the wettability depending on the surface energy of the solid, as Wenzel²³ and the Cassie-Baxter²⁴ models explain.

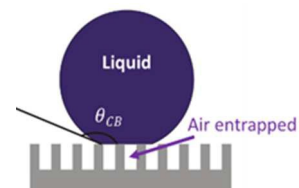
Particularly, the Cassie-Baxter equation²⁴ explains that the contact angle is increased as the fraction of the contact area between liquid and solid (solid fraction, f_s) is reduced. Known that the solid fraction f_s is a factor that explains the surface wettability in the Cassie-Baxter model,²⁴ efforts have been made to estimate the solid fraction, mostly by measuring the geometric dimensions of rough structures;^{6,16,25-26} however, direct observation of true solid fraction that a liquid is actually in contact with has not been made.

Cassie-Baxter equation: $\cos \theta_{CB} = f_s(\cos \theta_e + 1) - 1$

θ_{CB} : apparent contact angle for Cassie-Baxter state

θ_e (Young's contact angle): contact angle at smooth surface

f_s (solid fraction): area fraction where liquid is in contact with a solid surface



Kwon et al.¹¹ observed water droplets on a superhydrophobic fabric surface by an environmental scanning microscope (ESEM); however, the resolution of ESEM was not high enough to observe the interface between water and the fabric surface. Also, the water droplets on the surface were not stably positioned, and they rolled off the surface during the ESEM observation. In Park et al.'s study,¹⁶ the upper surface area of nano-pillars formed a superhydrophobic substrate was estimated, and the area fraction of the upper surface was used as the estimate of solid fraction, f_s . However, it is not the true representation of the surface that is in contact with liquid, and little evidence was provided whether this geometric estimate of roughness truly represented f_s . Often a low roll-off (or sliding) angle is suggested as an indirect evidence of the Cassie-Baxter's wetting state,²⁴ where a liquid is held by the entrapped air, thereby allowing an easy roll-off.²⁷ In this wetting state, the upper most area of a roughened substrate would be a close estimate of the contact area between the liquid and solid, which is f_s .

In our study, it was attempted to visually observe the solid area fraction where the liquid is actually in contact with, by employing fluorescence microscopy with a hydrophobic fluorescent dye, coumarin. The solid fraction observed by the fluorescence microscope was compared with the theoretical solid fraction calculated by the Cassie-Baxter equation, in order to examine the validity of the developed characterization method. To this end, superhydrophobic rough surfaces were fabricated via electrospinning and vapor coating processes. The wettability of the fabricated

surfaces was analyzed by contact angle and sliding angle measurements. The theoretical solid fraction, f_s , was calculated by the Cassie-Baxter equation²⁴ using the contact angles measured from both flat and rough surfaces. To visualize the predicted f_s on the surface, the gray-scale SEM images were converted into black-white binary images using a certain threshold of gray-scale so that the bright area fraction corresponds to the calculated f_s . To measure the actual solid fraction that is wet by water (f_s^{dye}), a drop of coumarin/water solution was rolled on the web surface; then the coumarin-adhered surface area was observed by a fluorescence microscope. The ultimate goal of this study is to develop a characterization method that allows direct observation of the solid fraction of the Cassie-Baxter model.²⁴ The schematic of image analysis and estimation of the solid fraction is shown in **Figure 1**.

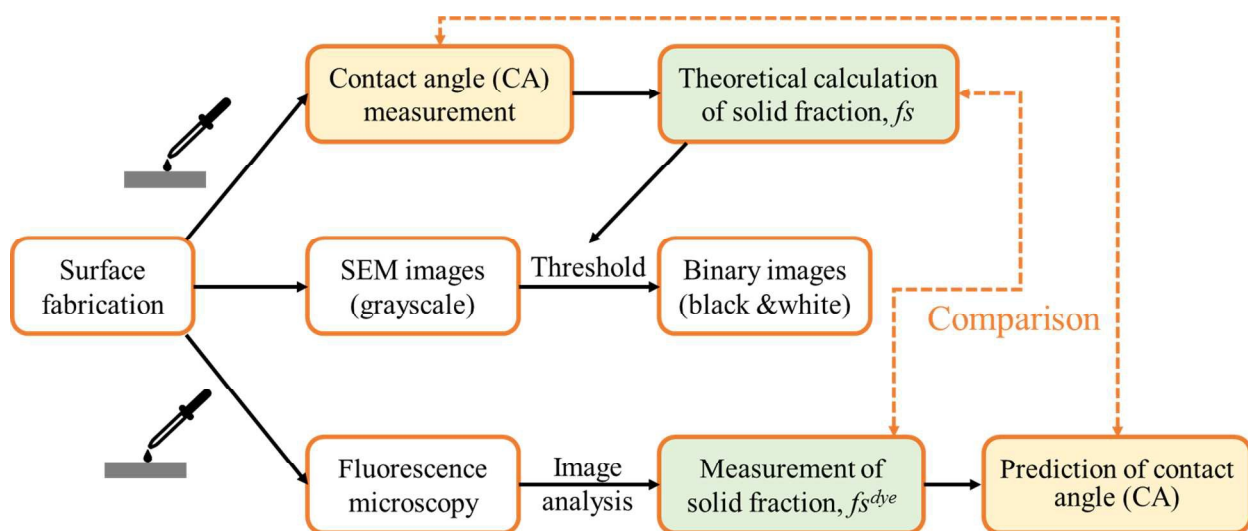


Figure 1. Process of image analysis, characterization of the solid fraction, and prediction of apparent contact angle.

2. Materials and Method

2.1. Materials

Polystyrene (PS) pellets (Mw 192,000, >99%) and ACS grade solvents including N, N-dimethylformamide (DMF), tetrahydrofuran (THF), methylene iodide (MI), isopropanol, acetone, and toluene were purchased from Sigma-Aldrich (USA). Coumarin 314 (99%, laser grade, ACROS Organics™) and n-hexane were purchased from Fisher Scientific (USA). 1H,1H,2H,2H-perfluorodecyltrichlorosilane (PFDTs) (96%) was purchased from Alfa Aesar (USA).

2.2. Fabrication of flat film and electrospun web

A PS film with a smooth and flat surface was prepared by a spin coater (VTC-100, MTI Corporation, USA) on a 2 cm × 4 cm glass slide. A 12 % (w/w) PS solution in toluene was prepared, and 1.2 mL of this solution was spin coated on a glass slide at 2000 rpm for 60 sec. The prepared sample was baked on a hotplate for 10 min at 110 °C to evaporate the solvent.

PS solutions of different concentrations (10 and 30 % w/w) were prepared in a mixture of THF (vapor pressure of 19,065 Pa) and DMF (vapor pressure of 516 Pa) with different volume ratios. The volume ratio of THF:DMF used are 0:4, 1:3, 2:2, and 3:1. The electrospinning setup (Spraybase[®], USA) consisted of a high voltage supply, a grounded aluminum drum-type collector, and a syringe pump. A 10 mL syringe with a 22-gauge needle and a polytetrafluoroethylene tubing (Kinesis, USA) were used to feed the PS solutions. The collector was placed in front of the needle at a distance of 10 cm, and fibers were spun horizontally toward the collector rotating at 100 rpm. The feeding rate of the PS solution was kept constant at 2.0 mL/hr throughout this study. The applied voltage was adjusted from 7 kV to 14 kV depending on polymer concentration and solvent mixture ratio. The electrospinning process was conducted at room temperature with 45±5 % relative humidity.

2.3. Surface modification

As to modify the surface energy, PS substrates were underwent air plasma treatment and/or vapor coating. The substrates were exposed to air plasma (PDC-32G, Harrick Plasma, USA), at approximately 100 mTorr, 18 W for 3 min. Through this treatment, -OH functional groups are formed on the surface, increasing the surface energy of the PS substrates. Also, this process facilitates the later process of PFDTs chemical attachment. To prevent the hydrophobic recovery of the plasma-treated substrates, samples were kept in distilled water immediately after the plasma treatment, and dried for 1 hr prior to further analysis or process.

To decrease the surface energy of PS substrates, PFDTs (surface energy of 17.2 mN/m) was deposited by a vapor coating process on the plasma-treated PS substrates. PFDTs was diluted to 5 % (v/v) in hexane, and 5 mL of the diluted solution was placed into a vacuum desiccator where the PS film or electrospun webs were placed. The pressure inside the desiccator was lowered to approximately 100 Torr, and the desiccator was kept at room temperature for 1 hr followed by being placed in an oven at 70 °C for 1 hr.²⁸ Chemical compositions of the PS substrates after air plasma treatment and PFDTs vapor coating were analyzed by Cary 630 FTIR-ATR spectrometer (Agilent Technologies, USA). Specimen codes for different substrates and processes are shown in **Table 1**.

Table 1. Specimen codes

Code	Description
F	Untreated spin-coated film
F _{pl}	Film treated by air plasma
F _{vc}	Film treated by air plasma followed by PFDTs vapor coating
E	Untreated electrospun web
E _{pl}	Electrospun web treated by air plasma
E _{vc}	Electrospun web treated by air plasma followed by PFDTs vapor coating

2.4. Contact angle measurement

Static contact angles (CA) and sliding angles (SA) were measured at room temperature by an optical tensiometer (Attension Theta, Biolin Scientific, USA). For CA measurement, 4 μL of distilled water (WA) was dropped vertically from 1 cm above the specimen surface, and the contact angle was measured after 1 sec. For sliding angle (SA) measurement, a specimen was fixed onto a stage, and a 10 μL water drop was placed on the specimen surface. The stage was tilted by 0.5° at a time, and the minimum tilting angle at which a water drop starts to roll away at least 1 cm was recorded as SA. For CA and SA, at least ten measurements were made from different locations of a specimen, and the mean value with standard deviation (SD) is presented. The theoretical solid fraction f_s of the Cassie-Baxter model²⁴ was calculated using the contact angles measured from a rough surface (electrospun web) and a flat surface (spin coated film).

2.5. Surface energy estimation

Surface energies of untreated PS film (F), PS film treated by air plasma (F_{pl}), and PS film treated by PFDTS (F_{vc}) were estimated by Wu's method²⁹, from the CAs measured for water and methylene iodide (MI). The polar (γ_L^p) and dispersive (γ_L^d) components, and the total surface tension (γ_L) for water and MI are as follows: for water, γ_L^p 51.0 mN/m, γ_L^d 21.8 mN/m, and γ_L 72.8 mN/m; for MI, γ_L^p 0 mN/m, γ_L^d 50.8 mN/m, and γ_L 50.8 mN/m.³⁰

2.6. Microscopic analysis

The morphology and surface roughness of the PS films and the electrospun webs were observed by a field-emission scanning electron microscope (FE-SEM) (Versa 3D Dual Beam, FEI, USA). Prior to SEM analysis, specimens were coated with Au/Pd in 20 nm thickness using a sputter coater (150TS, Quorum, UK).

Based on the solid fraction f_s that was calculated from the contact angle measurement, a black and white binary image from the SEM image was generated by adjusting the threshold of a gray-scale. For this image processing, ImageJ software (version 1.46r, NIH, USA) was used.

The actual contact area between water and the PS electrospun web was observed by a laser scanning confocal microscope (LSM 5 Pascal, Zeiss) with a hydrophobic fluorescent dye, coumarin 314. Though coumarin is a hydrophobic dye, a small amount is soluble in water (up to ~1.7 g/L). An aqueous solution with coumarin dye was prepared in a concentration of 0.73 g/L (~ 5 mM). A drop of the dye solution was rolled on an electrospun web and then removed from the surface. Due to the hydrophobic nature of coumarin, the hydrophobic PS surface was stained by coumarin when PS web was contacted by the aqueous coumarin solution. The surface area where coumarin adhered to was observed by a fluorescence microscope, and the area fraction of the fluoresced area (f_s^{dye}) was measured by ImageJ. For this analysis, at least four measurements of the fluorescence images per sample were used. This f_s^{dye} was regarded as the solid fraction where the water was actually in contact with. The f_s^{dye} was used to predict the apparent contact angle of the PS web, and the predicted CA was compared with the measured CA.

3. Results and Discussion

Influence of surface morphology on wettability

To investigate the influence of surface roughness on wettability, electrospun webs in different morphologies were produced by varying the concentration of PS solution and solvent mixing ratio (**Figure 2**). Beads were dominant at a lower polymer concentration (10 %) and fibrous forms were dominant at a higher polymer concentration (30 %). This morphological variation is attributed to the solution viscosity. When the viscosity of a solution is low (at low

concentration), a jet collapses into droplets before solvent evaporates, leading to beads formation.³¹ When the viscosity or polymer concentration reaches the critical point where chain entanglement occurs, jet breakup is prevented and uniform fibers can be produced.³²

Solvent volatility also affects the surface morphology. A highly evaporative solvent reduces the time to solidify polymers, generally giving a coarse surface.³³ Also, a mixture of solvents with different volatilities is reported to form pores or corrugations by the phase separation.³³⁻³⁴ In this study, DMF and THF were chosen as a less and more volatile solvent, respectively. With a higher ratio of DMF (THF:DMF of 0:4 and 1:3), fine pores or smooth surfaces were formed on beads and fibers. As the ratio of THF increases (3:1 THF:DMF), the surface of the beads or fibers became more corrugated or wrinkled. This phenomenon occurs when THF evaporates more quickly, forming a solid skin, while the core of the polymer solution is not solidified as quickly. With further solvent evaporation, the core loses the capability to support the skin, finally being collapsed and forming a wrinkled structure.³⁵ The results in **Figure 2** demonstrate that the morphology and roughness structure of the electrospun web can be controlled by polymer concentration and solvent mixing ratio.

Wettability of the produced webs was measured by water contact angles (CA) (**Figure 2**). Compared to the CA of the flat film (95°), CAs of the electrospun webs were considerably increased (139°~161°) due to the increased surface roughness by fine fibers and beads on the web. In general, beaded webs produced higher CAs than the uniform fiber webs.

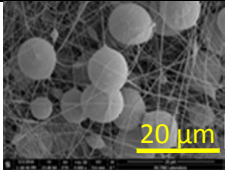
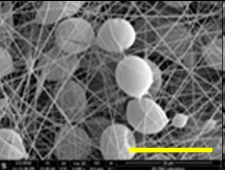
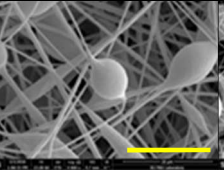
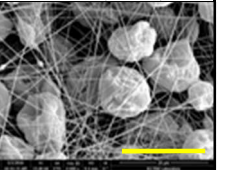
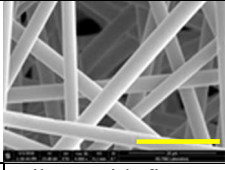
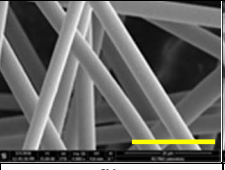
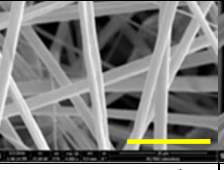
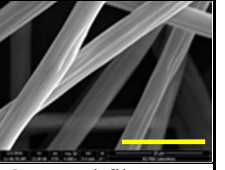
10% PS	THF:DMF (Voltage)	0:4 (10.5 kV)	1:3 (9.5 kV)	2:2 (9 kV)	3:1 (7 kV)
	CA ° (SD)	156° (±2.7)	151° (±2.3)	153° (±1.9)	161° (±2.6)
	SEM Image				
	Morphology	Porous beads on fine fibers	Porous beads on fine fibers	Beads on fine fibers	Wrinkled beads on fine fibers
30% PS	THF:DMF (Voltage)	0:4 (14 kV)	1:3 (14 kV)	2:2 (14 kV)	3:1 (14 kV)
	CA ° (SD)	139° (±2.7)	142° (±2.2)	144° (±2.5)	155° (±2.1)
	SEM Image				
	Morphology	Fibers with fine pores	Porous fibers	Porous, grooved fibers	Grooved fibers

Figure 2. Morphology of the PS electrospun webs produced from different conditions: water contact angle (CA) is presented by the mean value and standard deviation (SD).

* All inserted yellow bar represents a length of 20 μm .

Modification of surface energy

PS film (F) and electrospun web (E) were subjected to the chemical modifications to modify the surface energy. To increase the surface energy by oxidation, substrates were treated by air plasma. To decrease the surface energy, plasma-treated PS substrates were subjected to the chemical vapor deposition with PFDTS. Chemical compositions of the untreated PS and the modified PS surfaces were analyzed by FTIR (**Figure 3**). Bands of the FTIR spectrum for PS correspond to their aliphatic and aromatic C-H stretching in $2850\text{ cm}^{-1}\sim 3100\text{ cm}^{-1}$. After plasma treatment, bands in $1100\text{ cm}^{-1}\sim 1300\text{ cm}^{-1}$ appear, which correspond to C-O functional group. With the subsequent PFDTS vapor coating, the bands in $1000\text{ cm}^{-1}\sim 1300\text{ cm}^{-1}$ appear, resulting from the C-F stretching (PFDTS itself) and the chemical bonding between PS and PFDTS (Si-O-C stretching and Si-CH₃ bending). The peaks in spectra corroborate the presence of functional

groups that were introduced by the surface oxidation (by air plasma) and the hydrophobization (by PFDTS vapor coating).

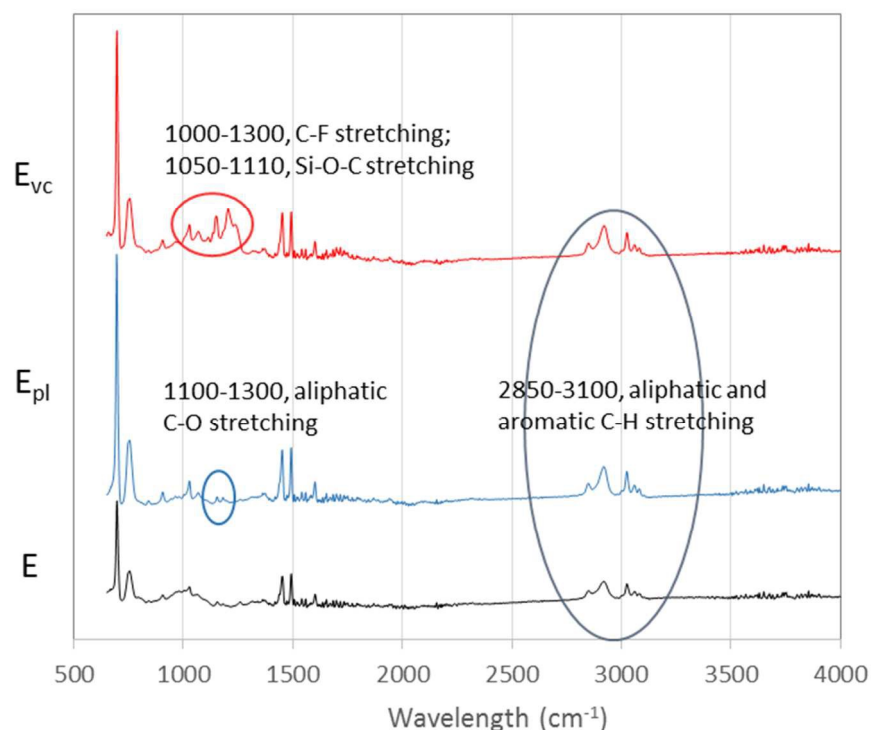


Figure 3. FTIR spectra of PS substrates: (a) untreated PS electrospun web, E; (b) PS web treated by air plasma, E_{pl} ; (c) PS web treated by air plasma followed by PFDTS vapor coating, E_{vc} .

The surface energy (SE) of a material was estimated using Wu's method²⁹. The estimated surface energy components of the film samples, F, F_{pl} , and F_{vc} , are presented in **Table 2** along with the CAs of water (WA) and methylene iodide (MI). Compared to the untreated PS substrate (SE 43.2 mN/m), the surface energy of the plasma treated substrate was considerably increased to 81.7 mN/m, while that of PFDTS coated was significantly reduced to 15.8 mN/m.

Table 2. Contact angle of water and methylene iodide, and the estimated surface energy

Specimen	Contact angle (°)		Surface energy (mN/m)		
	WA	MI	γ_s	γ_s^d	γ_s^p
F	95°	39°	43.2	40.6	2.6
F_{pl}	21°	18°	81.7	48.4	33.3
F_{vc}	115°	99°	15.8	13.6	2.2

* γ_S , surface energy of PS; γ_S^d , dispersive component of surface energy of PS; γ_S^p , polar component of surface energy; γ_L , surface tension of liquid; γ_L^d , dispersive component of surface tension of liquid; γ_L^p , polar component of surface tension of liquid.

* For water, γ_L 72.8 mN/m; γ_L^d 21.8 mN/m; γ_S^p 51.0 mN/m.³⁰

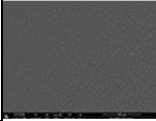
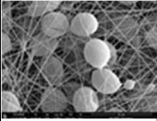
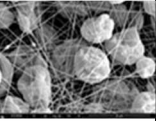
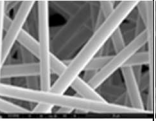
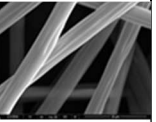
* For MI, γ_L 50.8 mN/m; γ_L^d 50.8 mN/m; γ_S^p 0 mN/m.³⁰

Combined effects of surface energy and morphology on wettability

Among the webs presented in **Figure 2**, two webs in a high CA range (10%-3:1, 30%-3:1), one web with the lowest CA (30%-0:4), and one web in between (10%-1:3) were selected to further analyze the effect of surface modification on the wettability (**Table 3**). When the surface was treated by air plasma, all electrospun webs (ES) were completely wet. With PFDTs coating, E_{vc} exhibited superhydrophobic property (water CA > 150°), while F_{vc} did not reach that level of hydrophobicity (CA~115°). From this result, it appears that there are limitations in achieving a superhydrophobic surface solely by lowering the surface energy, and the morphological parameters can have a substantial impact on anti-wettability.

When surface roughness is introduced to a low surface energy material, liquid is in contact with both the solid surface and the air pockets present between rough bumps, exhibiting the Cassie-Baxter state.²⁴ In this wetting state, the contact area between the liquid drop and solid surface is reduced, allowing an easy roll-off of droplets. The ability of roll-off is commonly evaluated by the sliding angle (SA) measurement; a lower sliding angle represents easier roll-off and higher anti-wettability. From F_{vc} surface, a water drop did not roll-off easily, and SA was not measurable. However, E_{vc} surfaces with beads and corrugated fibers exhibited low SAs (3°~3.5°). E_{vc} surfaces with smooth fibers gave relatively higher SAs (9°) (**Table 3**). From the SA measurements, it is speculated that the surface patterns such as beads and corrugations on the web are beneficial to reduce the contact area between water and solid surface, leading to the Cassie-Baxter²⁴ wetting state.

Table 3. Water contact angle (CA) and sliding angle (SA) of PS substrates with different surface modifications

	Film (F)	Electrospun webs (ES)			
PS conc. % (w/w)	12%	10%		30%	
THF:DMF	Toluene	1:3	3:1	0:4	3:1
SEM image					
CA untreated	95° (±1.1)	151° (±2.3)	161° (±2.6)	139° (±2.7)	155° (±2.1)
CA plasma-treated	21° (±1.4)	0° (all specimens were completely wet)			
CA vapor coated	115° (±1.6)	171° (±2.5)	172° (±2.0)	163° (±1.5)	169° (±3.5)
SA vapor coated	N/A	3.5° (±0.5)	3° (±0.3)	9° (±1.8)	3° (±0.5)

Analysis of solid fraction and prediction of wettability

For the analysis of solid fraction f_s in the Cassie-Baxter model,²⁴ three most anti-wetting surfaces from **Table 3** were chosen. With the presumption that the solid fraction f_s has a significant influence on the wettability, the Cassie-Baxter equation²⁴ explains the relationship between f_s , θ_e (Young's CA at a flat surface), and θ_{CB} (the apparent CA in Cassie-Baxter's wetting state) as follows:

$$\cos \theta_{CB} = f_s(\cos \theta_e + 1) - 1$$

The calculation of solid fraction f_s is based on the assumption that a water drop is in contact only with the upper area of the roughened surface, leaving the air pockets unwet. This assumption would be valid when a liquid with high surface tension is placed on a superhydrophobic surface without penetrating into the pores and roughening bumps.

Based on the theoretical assumption, we attempted to visualize the solid fraction f_s , or wet surface area, on SEM images ($\times 500$ magnifications). Since the protruded regions in the sample

have high chances of contacting with a water droplet and are brighter in SEM images, the protruded regions in the SEM images were segmented from the original SEM images by converting the gray-scale images into black and white binary images, using a threshold level so that the bright area fraction corresponds to the calculated f_s . In this procedure, the theoretical solid fraction f_s was calculated from the measured (apparent) contact angle and the Young's contact angle assuming the Cassie-Baxter state. The calculated f_s was then used as a reference value to set the threshold level to convert SEM images into binary images. The image processing was performed by ImageJ. The calculated f_s and the converted binary images are shown in **Figure 4**. Though this procedure does not provide an actual measurement of solid fraction, it suggests a way of visualizing or estimating the location of liquid-solid interfaces on the surface.

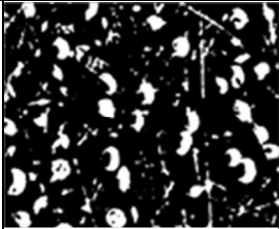

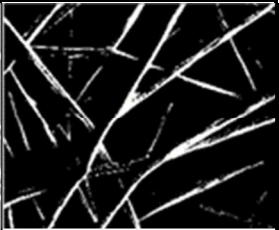



PS % (THF:DMF)	10% (3:1)	30% (0:4)	30% (3:1)
Untreated electrospun web (E)			
Binary image: bright area represents f_s			
f_s : calculated by the measured CAs of film and web	0.060	0.269	0.103
CA measured on specimen	161° (\pm 2.6)	139° (\pm 2.7)	155° (\pm 2.1)
Vapor coated electrospun web (E_{vc})			
Binary image: bright area represents f_s			
f_s : calculated by the measured CAs of film and web	0.017	0.076	0.032
CA measured on specimen	172° (\pm 2.0)	163° (\pm 1.5)	169° (\pm 3.5)

Figure 4. SEM binary images and f_s calculated from contact angles.

Of particular interest in this analysis is the solid area fraction of the beaded web. From the original gray-scale SEM image of the beaded web, it consists of both beads and fibers where beads were more protruded than fine fibers were. From the visualized solid fraction as appears white in the binary image, it was predicted that only the beads were in contact with water when the theoretical solid fractions were 6% and 1.7%.

The visualized wetted surface area would correspond well to the actual f_s if the wetted surface is flat and exhibits the Cassie-Baxter state (**Figure 5a**). In most cases, however, there would be discrepancies between the visualized and the actual wetted surface area, since this visualization process involves transformation of area from three-dimensional (3D) shapes into two-dimensional (2D) space. In the process of generating binary images in **Figure 4**, the predicted surface area from 3D shape (**Figure 5, ii**) was represented on 2D space, while keeping the same solid fractions (**Figure 5, i**). Thus, the wetted surface area appearing as white in the binary image (**Figure 4**) should be “stretched,” to accurately reflect the predicted solid fraction onto 2D space. Thereby, the visualized wetted surface area would be distorted and enlarged. The degree of discrepancy depends on the surface shape of the 3D structure, and errors or distortions that could occur during 3D to 2D transformation are illustrated in **Figure 5b**.

On the other hand, in the case of observing the surface area by fluorescence microscopy that will be demonstrated in the following section, the wetted surface area is the 2D projection of 3D topography. Therefore, f_s shown in the fluorescent image would be smaller than the actual f_s if the wetted surface is not flat (**Figure 5b, process from ii to iii**).

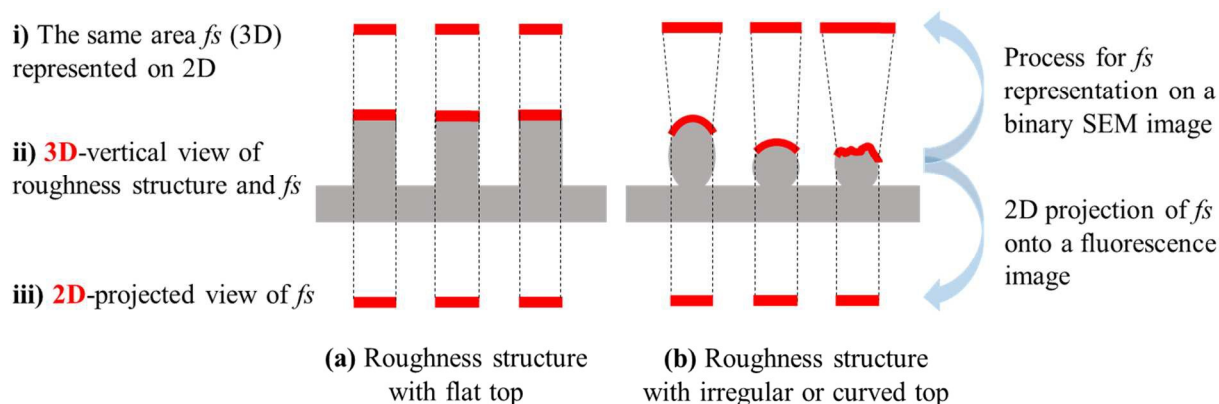


Figure 5. 3D and 2D representation of roughness and solid fraction f_s .

In order to investigate the actual solid fraction where the liquid is in contact with, a novel yet simple characterization method was developed. In this method, an aqueous solution with a hydrophobic fluorescent dye, coumarin, was prepared, and a drop of coumarin/water solution was rolled on the PS web surface. While a drop of the dye solution rolls on the PS web, the coumarin molecules adhered to the hydrophobic PS surface, and it allowed to trace the contact area between the liquid and the PS surface. The fluoresced area was observed by fluorescence microscopy. As the dye solution rolled on certain locations of the surface, the regions of microscopic images (mostly taken in $\times 500$ magnifications) were cropped to assure the whole area of selection was rolled over by the dye solution. The fraction of the fluoresced area from the image, f_s^{dye} , was measured by ImageJ and was regarded as the actual solid fraction contacted by water. In **Figure 6**, the solid fraction f_s^{dye} was observed by fluorescence microscopy, with the predicted contact angle (CA) from this f_s^{dye} value.

For the beaded webs, only a portion of the beads were stained by coumarin, indicating that the majority of the protruded structures in the web were beads. This fluorescent image is similar to the binary images in **Figure 4**, demonstrating the feasibility of this staining technique to be

applied to measure the actual wetted surface. For E_{vc} surfaces that showed superhydrophobic characteristics, f_s^{dye} and the predicted CAs corresponded fairly well with the theoretical f_s and the measured CAs, respectively. The prediction of CA was more accurate for superhydrophobic E_{vc} samples than less hydrophobic E samples. As E_{vc} samples ($CA \geq 169^\circ$, $SA \leq 3.5^\circ$) are more anti-wetting than E samples, the surfaces of E_{vc} would fit more closely with the Cassie-Baxter wetting state,²⁴ resulting in more accurate predictions. The CAs of the untreated electrospun webs were not as high as those of the vapor coated webs, and their wetting state may have been in transition between the Wenzel and the Cassie-Baxter states, in which the liquid is partially penetrated through the rough structures. It is also possible that the dye has not fully adhered to its contacted surface, underestimating the solid fraction especially for the highly repellent surfaces. Thus, an appropriate selection of a dye will be necessary for an accurate measurement of solid fraction.

As shown in **Figure 5**, when the coumarin-stained area from an irregular or curved surface is projected to a 2D microscopic image, the surface area could be underestimated than the actual surface area that was in contact with liquid. As the top most surface becomes flatter, the discrepancy between the actual f_s and the 2D-projected f_s becomes smaller. However, this tendency of underestimation of solid fraction on a 2D microscopic image is not clearly shown from the results in **Figure 6**.

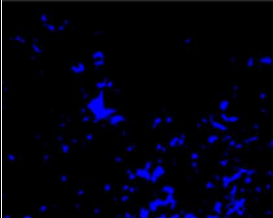
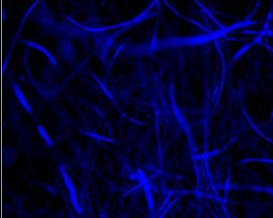
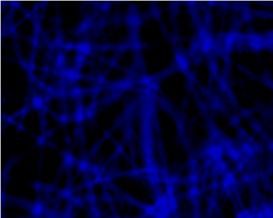
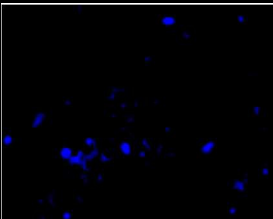
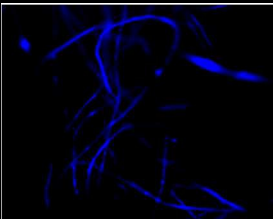
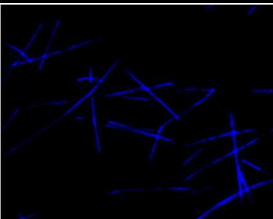
PS % (THF:DMF)	10% (3:1)	30% (0:4)	30% (3:1)
Untreated electrospun web (E)			
Fluorescence microscopy			
f_s^{dye} : measured from fluorescence area	0.060~0.073	0.199~0.307	0.095~0.178
θ^{dye} : predicted CA using f_s^{dye}	159°~161°	136°~145°	147°~156°
Vapor coated electrospun web (E_{vc})			
Fluorescence microscopy			
f_s^{dye} : measured from fluorescence area	0.015~0.032	0.068~0.078	0.029~0.036
θ^{dye} : predicted CA using f_s^{dye}	169°~172°	163°~164°	168°~170°

Figure 6. Fluorescent images for PS surfaces on which coumarin dye is adhered to: area fraction of bright area was measured as f_s^{dye} from the image (f_s^{dye} , solid fraction analyzed by the fluorescence images; θ^{dye} , apparent contact angle predicted with f_s^{dye}).

Seeing that the measured solid fraction by the staining method (**Figure 6**) roughly matches up with the theoretical value, we further examined whether the stained area corresponded well with the estimated solid area fraction from the binary image. For this comparison, the same area from a gray-scale bright field image and a fluorescent image was selected. Then, the selected area of the gray-scale image was converted into a binary image, using the theoretical f_s . The example of this comparison is shown for a beaded web, E_{vc} in **Figure 7**.

The stained area from the fluorescent image (f_s^{dye}) corresponded fairly well with the white

area on the binary image, which is the predicted f_s by the Cassie-Baxter model. In the fluorescent image (**Figure 7**, left), the solid fraction at the 3D surface was projected to the 2D microscopic image, and this projected area might underestimate the actual f_s (illustrated in **Figure 5**). In the binary image (**Figure 7**, right), the theoretical f_s was directly represented onto a 2D image, and this area may appear larger (or “stretched”) than the ones projected from 3D. This tendency is well presented in **Figure 7**. From the traced regions (numbered 1~8) of the matching images, the binary image consistently shows larger areas of spots (corresponds to **Figure 5b**, i) than the fluorescence microscopy image (corresponds to **Figure 5b**, iii).

The result from **Figure 7** demonstrates that the staining characterization method is valid to trace the actual solid fraction from a rough surface, and the binary image processing is a useful way of estimating the location of liquid-solid interfaces on a rough surface. Though this method was somewhat validated for the beaded surface, it was challenging to perform the same analysis for fibrous surfaces, because the bright field images for fibers had the light transmitted through the fibers, hindering the accurate depiction of fiber morphology in the desired gray-scale, which is necessary to generate clear binary images.

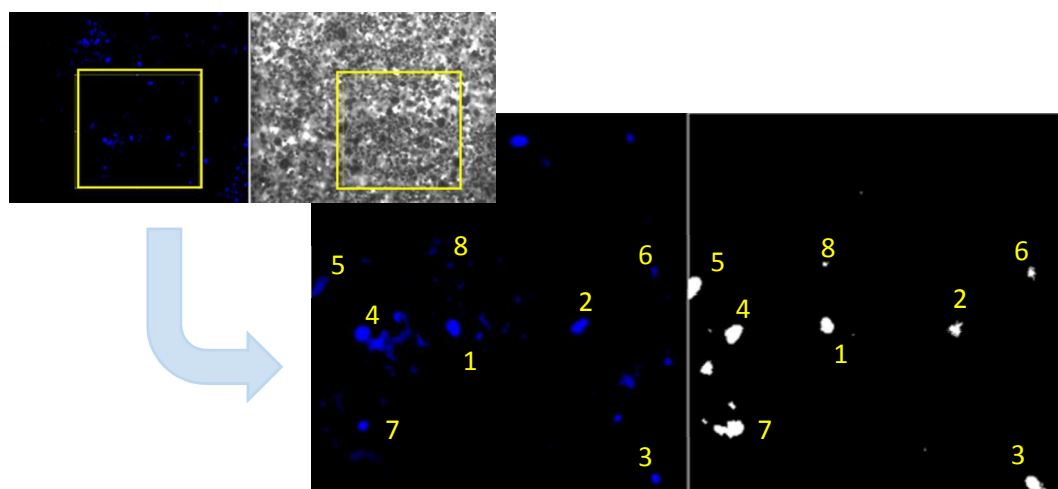


Figure 7. Comparison of fluorescence image (wet solid fraction is stained in blue) and binary image (predicted solid fraction is presented in white area).

The proposed characterization method will be useful to estimate the solid fraction and the apparent contact angle for the surface that follows the Cassie-Baxter state. However, further study is recommended to verify this method, by testing different surface structures with controlled and known geometric roughness. As illustrated in **Figure 4**, this characterization method will provide more accurate estimation of the wetting state for roughness with flat top (such as cylindrical pillars). To understand the possible distortion and errors of this characterization method, it is suggested to test this method on a standard roughness structure that exhibits the perfect Cassie-Baxter state. Also, this method gives only two-dimensional measurements. A method that allows the measurement of a three-dimensional interface will be beneficial for predicting the wettability that may not follow the Cassie-Baxter wetting state.

4. Conclusions

Superhydrophobic PS webs in different surface morphologies were produced via electrospinning and vapor coating processes. At a low concentration of the polymer solution (~10 %), beads were dominant, while fibrous forms were dominant at a high polymer concentration (~30 %). In a mixed solvent system with THF and DMF, rougher surfaces were formed due to phase separation. Compared to a flat film (CA 95°), electrospun webs (CA>139°) showed higher anti-wettability due to the surface roughness created by fibers and beads. Surface energy was modified to increase (75~82 mN/m) and to decrease (10~16 mN/m) by air-plasma and PFDTs coating, respectively. With PFDTs coating, the electrospun webs (E_{vc}) exhibited superhydrophobicity with $CA \geq 169^\circ$, while CA of the PFDTs coated film (F_{vc}) was 115° . E_{vc} also

exhibited low SAs ($\leq 3.5^\circ$), implying that the introduced roughness reduced the contact area between water and the solid surface, leading to the Cassie-Baxter²⁴ wetting state.

The theoretical solid fraction of the Cassie-Baxter model, f_s , was calculated from the measured CAs from the rough and flat surfaces. The gray-scale SEM images were converted into black and white binary images so that the bright area fraction matches up with the theoretically calculated f_s . This theoretical f_s was compared with the solid fraction that was visually observed (f_s^{dye}) by staining the hydrophobic surface with the hydrophobic fluorescence dye. The measured f_s^{dye} and the predicted CA by this f_s^{dye} value corresponded fairly well with the actual measurement of CA, especially for E_{vc} , of which surface appears to follow the Cassie-Baxter wetting state. However, when the actual solid fraction from the 3D surface is projected onto the 2D surface, the projected area may underestimate the solid fraction, f_s , for an irregular or curved roughness structure. Future study is recommended to validate the characterization method for various roughness structures and to develop an advanced characterization method that enables the visualization of wet surfaces in three dimensions to predict the wettability in various wetting states.

Acknowledgement

This work is supported by 3M Non-Tenured Faculty Grant; Johnson Cancer Research Center Innovation Research Award; University Small Research Grant (USRG) from the Kansas State University; and College of Human Ecology Sponsored research Overhead Awards (CHE-SRO) from the Kansas State University. Authors appreciate Dr. Daniel L. Boyle at the Microscopy Facility of Kansas State University for the help with fluorescence microscopy.

References

- 1 J. Genzer and K. Efimenko, Recent Developments in Superhydrophobic Surfaces and Their Relevance to Marine Fouling: A Review. *Biofouling*. 2006, **22**, 339-360.
- 2 Y. Lai, Y. Tang, J. Gong, D. Gong, L. Chi, C. Lin and Z. Chen, Transparent Superhydrophobic/Superhydrophilic TiO₂-based Coatings for Self-Cleaning and Anti-Fogging. *J. Mater. Chem.* 2012, **22**, 7420-7426.
- 3 Y. Lu, S. Sathasivam, J. Song, C.R. Crick, C.J. Carmalt and I.P. Parkin, Robust Self-Cleaning Surfaces that Function When Exposed to Either Air or Oil. *Science*. 2015, **347**, 1132-1135.
- 4 B. Leng, Z. Shao, G. de With and W. Ming, Superoleophobic Cotton Textiles. *Langmuir*. 2009, **25**, 2456-2460.
- 5 S. Pan, A.K. Kota, J.M. Mabry and A. Tuteja, Superomniphobic Surfaces for Effective Chemical Shielding. *J. Am. Chem. Soc.* 2013, **135**, 587-581.
- 6 A.K. Kota, W. Choi and A. Tuteja, Superhydrophobic Surfaces: Design and Durability. *MRS Bull.* 2013, **38**, 383-390.
- 7 T-S. Wong, T. Sun, L. Feng and J. Aizenberg, Interfacial Materials with Special Wettability. *MRS Bull.* 2013, **38**, 366-371.
- 8 S. Nishimoto and B. Bhushan, Bioinspired Self-Cleaning Surfaces with Superhydrophobicity, Superoleophobicity, and Superhydrophilicity. *RSC Adv.* 2013, **3**, 671-690.
- 9 A. Kota, J.M. Mabry and A. Tuteja, Superoleophobic Surfaces: Design Criteria and Recent Studies. *Surface Innovations*. 2013, **1**, 71-83.
- 10 T. Liu and C-J. Kim, Turning a Surface Superrepellent Even to Completely Wetting Liquids. *Science*. 2014, **346**, 1096-1100.

- 11 S-O. Kwon, T-J. Ko, E. Yu, J. Kim, M-W. Moon and C.H. Park, Nanostructured Self-Cleaning Lyocell Fabrics with Asymmetric Wettability and Moisture Absorbency (Part I). *RSC Adv.* 2014, **4**, 45442-45448.
- 12 J. Kim, H.S. Kim and C.H. Park, Contribution of Surface Energy and Roughness to the wettability of Polyamide 6 and Polypropylene Film in the Plasma-Induced Process. *Text. Res. J.* 2016, **86**, 461-471.
- 13 M. Kang, R. Jung, H-S. Kim and H-J. Jin, Preparation of Superhydrophobic Polystyrene Membranes by Electrospinning. *Colloids Surf. A.* 2008, **313-314**, 411-414.
- 14 I.Sas, R.E. Gorga, J.A. Joines and K.A. Thoney, Literature Review on Superhydrophobic Self-Cleaning Surfaces Produced by Electrospinning. *J. Polym. Sci. B Polym. Phys.* 2012, **50**, 824-845.
- 15 H-J. Choi, S. Choo, J-H. Shin, K-I. Kim and H. Lee, Fabrication of Superhydrophobic and Oleophobic Surfaces with Overhang Structure by Reverse Nanoimprint Lithography. *J. Phys. Chem.* 2013, **117**, 24354-24359.
- 16 Y. Park, C.H. Park and J.A. Kim, Quantitative Analysis on the Surface Roughness and the Level of Hydrophobicity for Superhydrophobic ZnO Nanorods Grown Textiles. *Tex. Res. J.* 2014, **84**, 1776-1788.
- 17 B. Shin, K-R. Lee and M-W. Moon, Extreme Water Repellency of Nanostructured Low-Surface-Energy Nonwoven Fabrics. *Soft Matter.* 2012, **8**, 1817-1823.
- 18 T-J. Ko, E.K. Her, B. Shin, H-Y, Kim, K-R. Lee and B.K. Hong, Water Condensation Behavior on the Surface of a Network of Superhydrophobic Carbon Fibers with High-Aspect-Ratio Nanostructures. *Carbon.* 2012, **50**, 5085-5092.

- 19 C-H. Xue, Y-R. Li, P. Zhang, J-Z. Ma and S-T. Jia, Washable and Water-Resistant Superhydrophobic Surfaces with Self-Cleaning Property by Chemical Etching of Fibers and Hydrophobization. *ACS Appl. Mater. Interfaces*. 2014, **6**, 10153-10161.
- 20 J. Lin, B. Ding, J. Yu and Y. Hsieh, Direct Fabrication of Highly Nanoporous Polystyrene Fibers via Electrospinning. *ACS Appl. Mater. Interfaces*. 2010, **2**, 521-528.
- 21 M. Nosonovsky and B. Bhushan, Superhydrophobic Surfaces and Emerging Applications: Non-Adhesion, Energy, green Engineering. *Curr. Opin. Colloid Interface Sci*. 2009, **14**, 270-280.
- 22 T. Young, An Essay on the Cohesion of Fluids. *Phil. Trans. R.Soc. Lond*. 1805, **95**, 65-87.
- 23 R.N. Wenzel, Resistance of Solid Surfaces to Wetting by Water. *Ind. Eng. Chem*. 1936, **28**, 988-994.
- 24 A. Cassie and S. Baxter, Wettability of Porous Surfaces. *T. Faraday Soc*. 1944, **40**, 546-551.
- 25 Y. Rahmawan, M.W. Moon, K.S. Kim, K.R. Lee and K.Y. Suh, Wrinkled, Dual-Scale Structure of Diamond-Like Carbon (DLC) for Superhydrophobicity. *Langmuir*. 2010, **26**, 484-491.
- 26 T.G. Cha, J.W. Yi, M-W. Moon, K-R. Lee and H-Y. Kim, Nanoscale Patterning of Microtextured Surfaces to Control Superhydrophobic Robustness. *Langmuir*. 2010, **26**, 8319-8326.
- 27 S. Park, J. Kim and C.H. Park, Analysis of wetting state for super-repellent fabrics to liquids in varied surface tensions. *RSC Adv*. 2016, **6**, 45884-45893.
- 28 Z. Pan, H. Shahsavan, W. Zhang, F-K. Yang and B. Zhao, Superhydro-oleophobic bio-inspired polydimethylsiloxane micropillared surface via FDTS coating/blending approaches. *Appl. Surf. Sci*. 2014, **324**, 612-620.

- 29 S. Wu, Calculation of interfacial tension in polymer system. *J. Polym.Sci., Polym. Symp.* 1971, **34**, 19-30.
- 30 M. Żenkiewicz, Methods for the Calculation of Surface Free Energy of Solids. *J. Achiev. Mater. Manuf. Eng.* 2007, **24**, 137-145.
- 31 A. Frenot and I.S. Chronakis, Polymer Nanofibers Assembled by Electrospinning. *Curr. Opin. Colloid Interface Sci.* 2003, **8**, 64-75.
- 32 P. Gupta, C. Elkins, E.L. Timothy and G.L. Wilkes, Electrospinning of Linear homopolymers of Poly(methylmethacrylate): Exploring Relationships between Fiber Formation, Viscosity, Molecular Weight and Concentration in a Good Solvent. *Polymer.* 2005, **46**, 4799-4810.
- 33 T. Subbiah, G.S. Bhat, R.W. Tock, S. Parameswaran and S.S. Ramkumar, Electrospinning of Nanofibers. *J. Appl. Polym. Sci.* 2005, **96**, 557-569.
- 34 Z. Qi, H. Yu, Y. Chen and M. Zhu, Highly Porous Fibers Prepared by Electrospinning a Ternary System of Nonsolvent/Solvent/Poly(L-lactic acid). *Mater. Lett.* 2009, **63**, 415-418.
- 35 K.A.G. Katsogiannis, G.T. Vladislavljevic and S. Georgiadou, Porous Electrospun Polycaprolactone (PCL) Fibres by Phase Separation. *Eur. Polym. J.* 2015, **69**, 284-295.